AIAA Propulsion and Energy Forum
July 28-30, 2014, Cleveland, OH
50th AIAA/ASME/SAE/ASEE Joint Propulsion Conference

10.2514/6.2014-3710

The Effect of Background Pressure on SPT-100 Hall Thruster Performance

Kevin D. Diamant[1]
The Aerospace Corporation, El Segundo, CA, 90245

Raymond Liang[2] and Ronald L. Corey[3]
SSL, Palo Alto, CA, 94303

A flight-model SPT-100 Hall thruster from the Fakel Experimental and Design Bureau was characterized with respect to performance and plume properties at The Aerospace Corporation and at L-3 Electron Technologies, Inc. over vacuum facility background pressures ranging from 2.3×10^{-4} to 9.5×10^{-3} Pa (1.7×10^{-6} to 7.1×10^{-5} Torr). Thrust and xenon mass flow rate measured at both facilities agreed to within the measurement uncertainties. Thrust decayed exponentially, while flow rate increased linearly with decreasing pressure. Using simple curve-fits for extrapolation, thrust, specific impulse, efficiency, and flow rate were projected to change by -4, -10, -14, and 7% respectively at zero pressure relative to 6.7×10^{-3} Pa (5.0×10^{-5} Torr). A decrease in net ion accelerating voltage and an increase in plume divergence were identified as contributors to decreased thrust with decreasing pressure. The amplitude of discharge current oscillations decreased linearly with decreasing background pressure, while the center frequency of the oscillations also decreased, from 26 to 16.5 kHz, but in non-linear fashion. Neutral density near the exit plane of Hall thrusters can be quite low, $O(10^{18})$ m^{-3}, such that background neutrals from the residual gas in the vacuum chamber may significantly influence ionization and conduction there.

I. Introduction

VACUUM facility background pressure has been shown to affect Hall thruster performance, erosion rates, and internal plasma properties.[1-8] In this study, a flight-model SPT-100 Hall thruster (serial number 27) from the Fakel Experimental and Design Bureau (Fakel) was characterized with respect to performance and angle-dependent ion flux and ion energy at The Aerospace Corporation (Aerospace) and at L-3 Communications Electron Technologies, Inc. (L-3) over background pressures ranging from 2.3×10^{-4} to 9.5×10^{-3} Pa (1.7×10^{-6} to 7.1×10^{-5} Torr).

SPT-100s started flying on Russian satellites in 1994. A decade later they entered service on Western satellites built by Space Systems/Loral and Astrium.[9] To date, approximately 200 SPT-100s have flown, with reports indicating nominal performance in orbit.[9-13]

The SPT-100 was qualified for flight on Western spacecraft through testing in the 1990s at Fakel,[14-16] at the NASA Glenn Research Center,[17] and at the Jet Propulsion Laboratory.[18] Between them, they covered vacuum facility background pressures ranging from 4.3×10^{-4} to 7.5×10^{-3} Pa (3.2×10^{-6} to 5.6×10^{-5} Torr), however it is not clear that trends in thruster performance as a function of background pressure can be reliably established from those tests since the same thruster and cathode flow fraction were not used in all cases. Also, background pressure measurements might not be transportable between facilities, due to variations in the type and location of the pressure gauges. In this work, the same pressure gauge mounted in approximately the same location relative to the thruster was used to measure background pressure at both facilities.

II. Experimental Apparatus

A. Vacuum facilities

The Aerospace vacuum facility is a 2.4 m diameter by 9.8 m long cryopumped vacuum chamber with a maximum measured xenon pumping speed of approximately 250 kl/s. Two re-entrant cryopumps were on the chamber end dome behind the thruster, four re-entrant pumps were in the beam dump region, and four 1.2 m diameter cryotubs were mounted on the cylindrical wall of the chamber adjacent to the thruster (Fig. 1). Vacuum facility background pressures were measured with an internally mounted, metal-encapsulated "Stabil-ion" ionization

[1] Research Scientist, Propulsion Science, 2310 E. El Segundo Blvd, M2-341, AIAA Senior Member.
[2] Senior R&D Engineer, Propulsion Products, 3825 Fabian Way, MS G-86, AIAA Member.
[3] Mechanical Engineering Specialist, Propulsion Products, 3825 Fabian Way, MS G-86, AIAA Member.

gauge (labeled "Internal IG" in Fig. 1). The gauge was mounted on a 2-3/4 inch conflat "tee" so that ingested plasma would have to make a right-angle turn, and presumably be neutralized by wall collisions, before reaching the gauge (Fig. 2a). The entrance aperture to the tee was equipped with two wire-mesh grids with approximately 25 micron apertures. The first grid could be biased to repel electrons, and the second to repel ions, however it was found experimentally that grid biasing affected pressure readings by approximately 1% relative to the unbiased case, and so the grids were left floating. The gauge was calibrated in air against a NIST-traceable standard (spinning rotor gauge), and was found to differ from the standard by 5% or less over the range of pressures reported here. The gauge was mounted with the tee entrance aperture facing in the same direction as the thruster exit plane. This orientation ensured that directed neutral flux, such as could arise from a pressure gradient in the vacuum chamber, would enter the gauge as it would the thruster. The centerline of the tee entrance aperture was located 19 cm radially from thruster centerline at approximately the 9 o'clock position when facing the thruster exit plane, and the plane of the entrance aperture was 10 cm behind the thruster exit plane.

Testing at L-3 occurred in the 6.1 m diameter by 12.2 m long vacuum chamber that was built for life testing of the 25 cm XIPS ion engine.[19] This chamber is equipped with 30 externally-mounted 1.2 m diameter cryotubs. The same ionization gauge assembly described in the preceding paragraph was taken to L-3 and used to measure vacuum chamber background pressures. As at Aerospace, the assembly was mounted with the entrance aperture facing in the same direction as the thruster exit plane. The entrance aperture centerline was located 16.5 cm radially from thruster centerline at approximately the 10 o'clock position when facing the thruster exit plane, and the plane of the entrance aperture was 10 cm behind the thruster exit plane (Fig. 2b).

Background pressure was varied at both facilities through a combination of varying the number of active pumps and by injecting excess xenon. At Aerospace the excess xenon was injected through a port located on the chamber wall at chamber centerline and approximately 1.4 m downstream of the thruster exit plane. At L-3 the excess xenon port was on the chamber wall near the base of the chamber at approximately the same axial location as the thruster.

Both facilities also had ionization gauges mounted on the chamber wall at approximately the same axial location as the thruster. It is interesting to note that the wall-mounted gauge at Aerospace gave readings that were from 2 to 30% smaller than those from the internally mounted gauge, while at L-3 the wall-mounted gauge readings were from 2% smaller to 66% larger than the internal gauge readings, depending on how many pumps were operating and whether or not excess xenon was supplied. It is also noteworthy that, at Aerospace, the internally mounted gauge was rotated about an axis coincident with the plane of the tee entrance aperture, presumably allowing the static pressure to be sampled at a fixed location while observing variations in "dynamic" pressure. It was found that facing the entrance aperture upstream (i.e., opposite to the direction faced by the thruster) caused the gauge readings to decrease by as much as 70% at the lowest operating pressures (~ 1×10^{-5} Torr), indicating the presence of a directed flux of neutrals flowing toward the thruster exit plane. All pressures reported in this document are from the internally mounted gauge, facing downstream and positioned as described in the preceding paragraphs.

Ionization gauge readings were corrected using the scale factor of 0.348 specified by the gauge manufacturer for xenon relative to nitrogen.

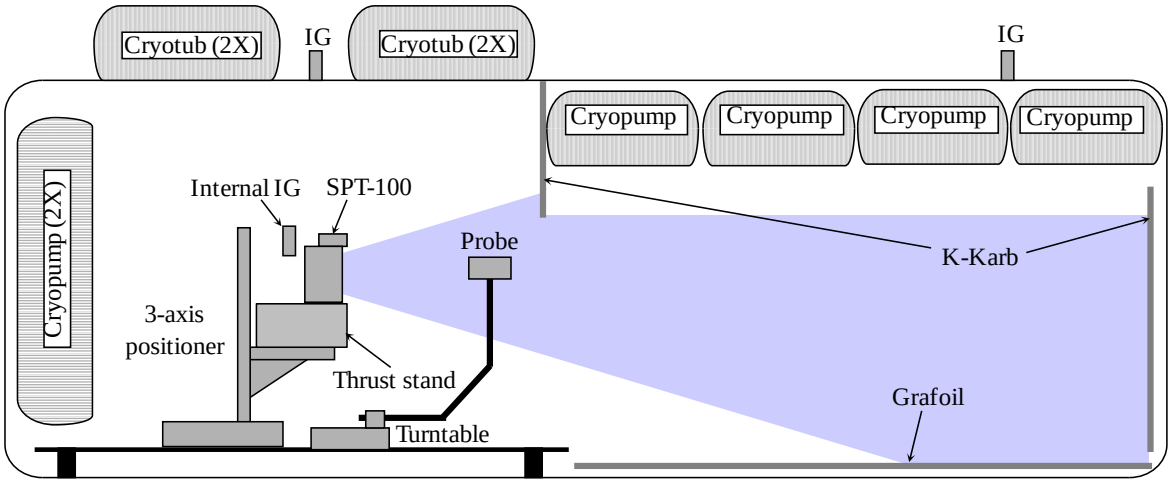

Figure 1. Schematic of Aerospace vacuum facility. IG = ionization gauge for measurement of background pressure. Pressures reported in this document were measured by the "Internal IG."

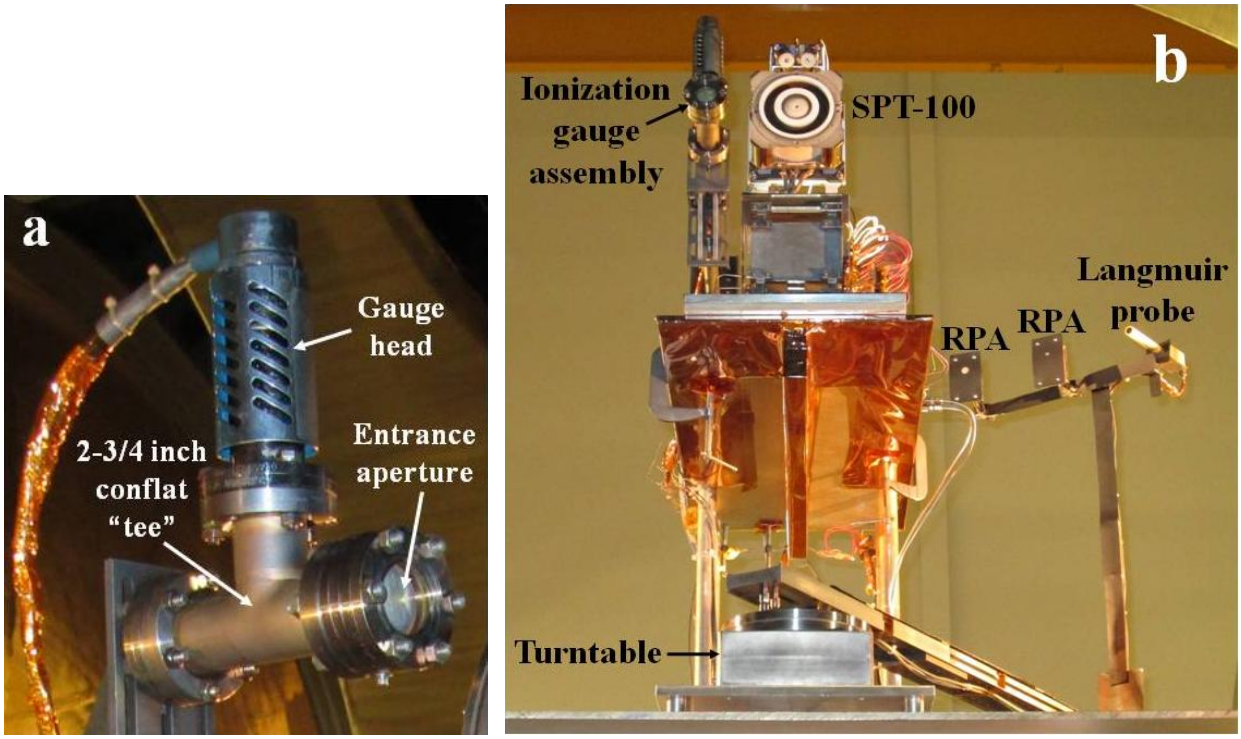

Figure 2. a) Internal ionization gauge assembly. b) SPT-100 at L-3, showing internal ionization gauge assembly, thrust stand, and plume probes. The retarding potential analyzer (RPA) at the center of the probe rake was not used. The cathode on the right in the photo was used exclusively at both Aerospace and L-3.

B. Thruster operation

The SPT-100 was operated at a constant discharge voltage of 300 V and constant discharge power of 1.35 kW. As background pressure was varied, the total xenon flow rate was adjusted to maintain a discharge current of 4.50 A. The flow rate to the cathode was adjusted to maintain an anode-to-cathode flow rate ratio of 12:1. Each facility had its own xenon feed system and thermal mass flow controllers. The mass flow controllers were calibrated in place at both facilities by timing the rate of pressure rise while flowing into a one-liter fixed volume.

The thruster was run with laboratory power supplies. The discharge supply was equipped with the filter shown schematically in Fig. 3. The SPT-100 electromagnets are wired in series with the discharge. In addition, a "magnet augment" current of 1.5 A was supplied, yielding a total magnet current of 6.0 A.

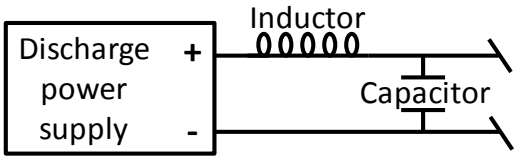

Figure 3. Schematic of discharge filter. The capacitor value was 5.6 μF, while the inductor was 339 μH at Aerospace and 215 μH at L-3.

C. Diagnostics

1. Thrust stand

The Aerospace thrust stand was used at both facilities. It is an inverted-pendulum style stand equipped with load cells for direct thrust measurement (Fig. 4). The sensing element of the thrust-measuring load cell ("thrust sensor") supported the pendulum against horizontal motion. A second load cell ("calibration sensor") was mounted behind the thruster, and was connected via nylon line and a spring to a stepping motor mounted to the stationary base of the

pendulum. Thrust was measured by recording the difference between thrust sensor outputs with the thruster on and off ("off" means no power or propellant flow). Calibrations were performed with the thruster off by recording the response of the thrust sensor to a series of loads applied to the calibration sensor by applying tension to the spring. At Aerospace, the thrust stand was calibrated following every two thrust measurements, and typically at least 8 measurements were taken at each operating condition and averaged. At L-3, the thrust stand was calibrated after every measurement, and typically 3 measurements were averaged at each operating condition.

At both facilities the vacuum chamber was connected to a dedicated ground terminal. At Aerospace the thruster mounting structure and thrust stand were electrically connected to the vacuum chamber. At L-3 the mounting structure and thrust stand were electrically isolated from the vacuum chamber and from each other. Each was connected to a wire running outside the vacuum chamber that allowed them to be grounded if desired. All of the L-3 thrust measurements reported here were taken with the thruster and thrust stand electrically isolated from the vacuum chamber and from each other. At various times the thruster and thrust stand were grounded independently or together and no change in thrust larger than the thrust stand background noise, which was typically ≤ 0.5 mN, was ever observed.

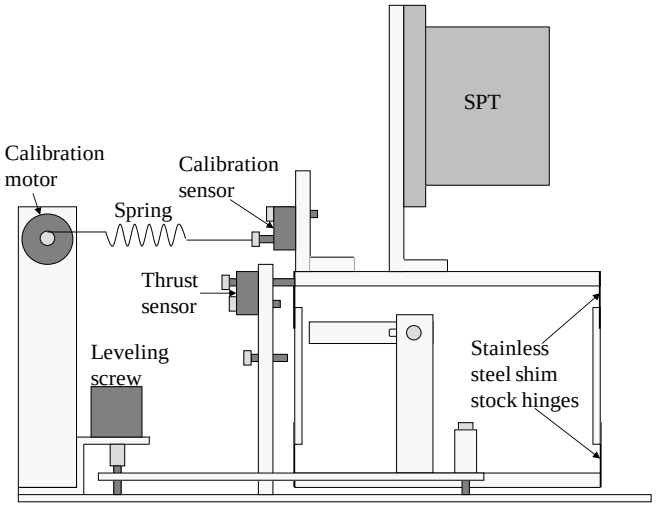

Figure 4. Schematic of thrust stand.

2. Discharge current

Discharge current time histories were recorded with an oscilloscope at a sampling frequency of 500 kHz with a total recording period of 20 ms, corresponding to a Nyquist frequency of 250 kHz and frequency resolution of 25 Hz. The current probe was located on the anode line on the thruster side of the discharge filter. Values of "discharge current noise" reported here were calculated by taking the ratio of the standard deviation of the current to its average value.

3. Plume probes

Single-electrode, planar Langmuir probes were used at both facilities. At Aerospace a 2.54 cm diameter stainless steel collector was used, while at L-3 we used a 1.35 cm diameter Kovar collector (Fig. 2b). Current was recorded as the probe voltage was swept from -20 V to 20 V relative to ground in increments of 0.2 V. Plasma potential was identified as the voltage at which the slope of the current-voltage (I-V) curve attained its maximum value. The ion current collected at plasma potential was estimated by generating a linear fit to the ion-saturation portion of the I-V curve, and extrapolating to plasma potential. Electron current vs. voltage at or below plasma potential was obtained by subtracting the estimated ion current (from the linear fit) from the total current. Electron temperature was derived from the slope of a semi-logarithmic plot of the electron I-V curve, and electron density was obtained from the electron current measured at plasma potential using the following expression:

$$n_e = \frac{I_{eo}}{q^{3/2} A} \left(\frac{2\pi m_e}{T_e} \right)^{1/2} \tag{1}$$

where n_e is the electron density, I_{eo} is the electron current at plasma potential, q is the elementary charge, A is the geometric probe collection area, m_e is the electron mass, and T_e is the electron temperature in eV.

A retarding potential analyzer (RPA) was used to measure ion flux and energy distributions at L-3 only (Fig. 2b). The RPA and associated circuit are shown schematically in Fig. 5. The entrance aperture to the negatively-biased enclosure was covered by a pair of electron-repelling mesh grids that were in electrical contact with the enclosure. These were followed by an ion-repelling grid ("repeller"), then an aluminum collector. The mesh grids were made from 316 stainless steel wire cloth with a wire diameter of 25 μm (0.001 in), opening size of 38 μm (0.0015 in), and geometrical open-area fraction of 38%. The collector bias was ramped along with that of the repeller by tying the repeller either directly to the "guard" output of the sourcemeter (the "guard" output is designed to provide the same voltage, to within millivolts, as the "Hi" output, but current collected on the guard does not pass through the internal ammeter), or to the positive terminal of an 18.3 V battery placed between the repeller and guard as shown in Fig. 6. This procedure is thought to have the following advantages. Biasing the collector at a potential close to that of the repeller reduced the likelihood of an electrical discharge between the two, and improved the uniformity of the potential over the surface of the repeller, thereby reducing false broadening of the ion energy distribution. At large positive values of repeller bias, net electron collection was in some cases observed when the repeller was tied directly to the guard output. Inserting the battery provided a small negative bias on the collector relative to the repeller and eliminated net electron collection.

Ion "flux" measurements were made with the RPA by biasing the repeller from -20 to 100 V relative to ground in 20 V increments at each angular location. The repeller bias was varied from 0 to 400 V relative to ground in 2 V increments for measurements of the ion energy distribution.

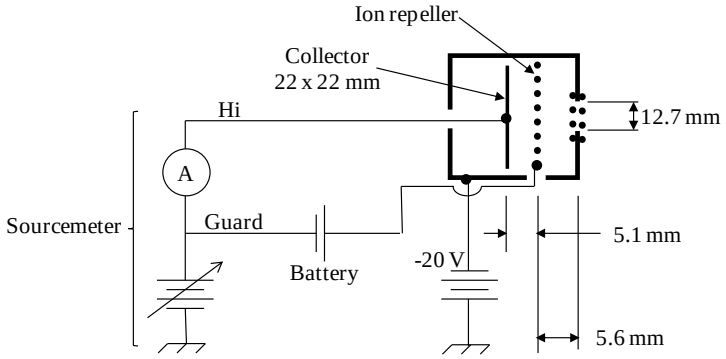

Figure 5. Retarding potential analyzer (RPA) and associated power supplies.

III. Results

A. Performance

Figure 6 shows results for thrust F, specific impulse I_{sp}, efficiency η, and xenon mass flow rate $\dot{m}$ as functions of background pressure. Specific impulse and efficiency are defined as:

$$I_{sp} = \frac{F}{\dot{m}g} \tag{2}$$

$$\eta = \frac{F^2}{2\dot{m}(J_D V_D + P_{mag})} \tag{3}$$

where g is Earth's sea-level gravitational acceleration, J_D is the discharge current, V_D is the discharge voltage, and P_{mag} is the magnet augment power. The functional forms of the curvefits in Fig. 6 are not physics-based, but were selected for simplicity while maintaining a fit to the experimental data that is pleasing to the eye. Table 1 shows very good agreement between SPT-100 performance parameters averaged over the life test performed at Fakel[16] at a background pressure of 6.7×10^{-3} Pa (5.0×10^{-5} Torr), and values obtained by interpolation of the Aerospace/L-3 data using the curvefits shown in Fig. 6. Also shown in Table 1 are the projected performance parameters at zero background pressure, and the percentage differences between performance parameters at 5.0×10^{-5} Torr and zero background pressure, again using the curvefits from Fig. 6 for interpolation and extrapolation.

Thrust measurement uncertainty was dominated by the repeatability of thrust stand calibrations, and was estimated to be 0.7% at Aerospace and 0.9% at L-3. Xenon mass flow rate measurement uncertainty was estimated to be 0.8% at both facilities. We adopted the conservative approach of summing the uncertainties of each parameter

in a product or quotient to obtain estimated uncertainties of 1.5% and 2.2% for specific impulse and efficiency respectively at Aerospace, and 1.7% and 2.6% respectively at L-3.

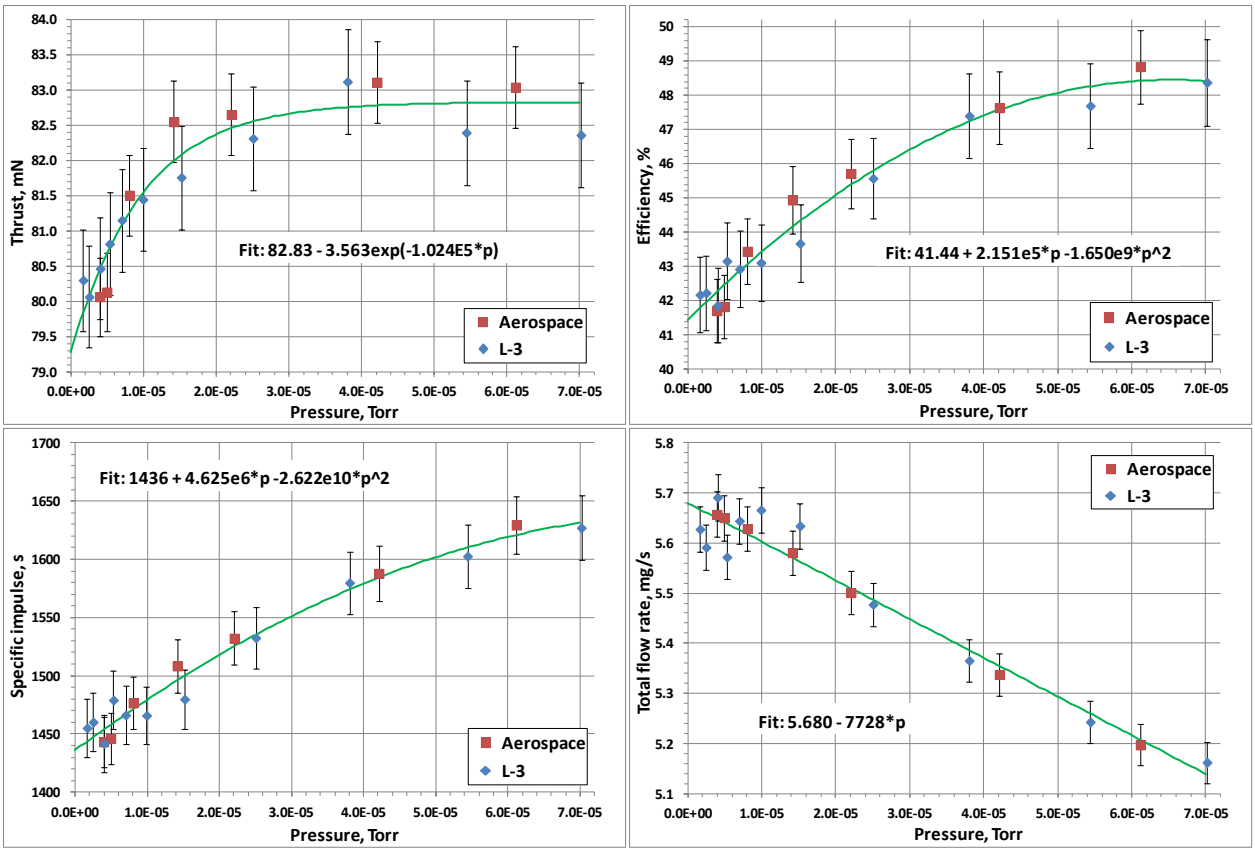

Figure 6. SPT-100 performance. In curvefits, "p" is the pressure in Torr.

Table 1. Performance comparison and extrapolation to vacuum.

				Δ from
				5E-5 Torr
	5E-5 Torr			to 0 Torr
	life test	5E-5 Torr	0 Torr	Aero/L-3
	Fakel[16]	Aero/L-3	Aero/L-3	(%)
Thrust (mN)	83.9	82.8	79.3	-4.3
Isp (s)	1570	1602	1436	-10.3
Efficiency (%)	48	48.1	41.4	-13.8
Flow rate (mg/s)	5.45	5.29	5.68	7.3

B. Discharge stability

The plot on the left in Fig. 7 shows that the discharge current noise decreased almost linearly with decreasing pressure, from approximately 10 to 4%. Fourier transforms of the discharge current time histories revealed that the bulk of the discharge current oscillations formed a broad peak centered within the frequency range often associated with the so-called "breathing" mode instability. The center frequency of these oscillations decreased with decreasing pressure from approximately 26 to 16.5 kHz in non-linear fashion, as shown in the plot on the right in Fig. 7. The breathing mode oscillation frequency is thought to scale inversely with the neutral transit time across the "zone of ionization," [20] so the data in Fig. 7 may indicate a widening of the ionization zone or a reduction in neutral velocity, or, more generally, an increase in the time required to replenish neutrals in the ionization zone as pressure decreased.

Error bars are not shown in Fig. 7 since typically only one or two oscilloscope recordings were made at each operating condition, precluding statistical estimation of measurement uncertainties.

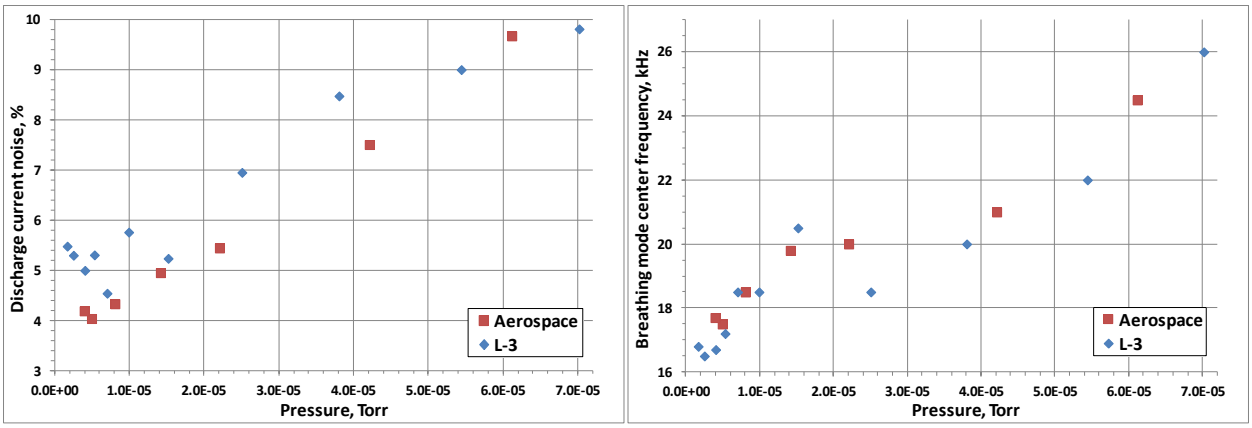

Figure 7. Discharge current stability and frequency of the breathing mode.

C. Plume properties

1. Electron temperature, density, and plasma potential

Figure 8 shows plasma potential with respect to ground, electron temperature, and electron density as functions of angle from thruster centerline (5° resolution) at a radius of 100 cm. Electron temperature generally increased with decreasing background pressure, possibly in part due to a reduced rate of inelastic collisions between electrons and background neutrals. This explanation, however, does not account for the reduction in electron temperature observed at the three lowest pressures at angles greater than 50° at L-3. Those data may indicate the presence of a more complex interaction possibly involving neutrals and the cathode-to-plume potential drop that energizes plume electrons. In any case, it is likely that the increase in electron temperature accounts for the observed increase in plasma potential (with respect to ground) in the core of the plume as background pressure decreased since the ambipolar electric field that enforces plume quasineutrality is proportional to electron temperature. Increased electron density with increasing background pressure presumably resulted from an increasing population of slow ions produced by charge exchange and elastic collisions of primary ions with background neutrals, and by electron-impact ionization of background neutrals.

Results from Aerospace and L-3 are qualitatively very similar (note that the background pressures associated with the various curves are not identical between facilities). The most obvious differences occurred with electron temperatures at angles greater than approximately 30°. We can speculate that these differences resulted from differences in the spatial distribution of background neutrals between the two facilities.

Estimated uncertainties for the Langmuir probe data are 0.2 V for plasma potential, 20% for electron temperature, and 30% for electron density.

2. Ion flux

Figure 9 shows ion flux recorded at L-3 with the RPA and Langmuir probe as a function of angle (5° resolution) from thruster centerline at a radius of 100 cm (some data were lost at 5.51E-5 Torr due to a malfunction of the sourcemeter that was not detected in time to repeat the measurement). Data from the RPA are labeled "RPA X," where X is the ion-repelling bias with respect to ground (i.e., only ions with energy-to-charge ratios greater than X were collected). Data labeled "Langmuir -20" were recorded with a -20 V bias with respect to ground, and those labeled "Langmuir pp" were determined from ion currents obtained by extrapolating Langmuir ion saturation current data to plasma potential, as described in Section II.C.3. The effective ion collection area of the RPA was determined for each operating condition (power and background pressure) as the value that would minimize the sum of the squares of the differences between the RPA flux data and the Langmuir flux data when both were biased to -20 V. This procedure resulted in values for the ion transparency of the RPA mesh grids between 32 and 34%, in good agreement with Ref. 21, in which a transparency of 33% was reported using the same mesh. Langmuir and RPA flux data at -20 V diverged with increasing angle due to the smaller field-of-view of the RPA, which discriminated against low energy ions created in the extended source volume of the plume (by charge exchange or

elastic collisions between ions and neutrals, or by ionization of neutrals by electron impact) and which approached the probes at highly non-normal incidence.

The data in Fig. 9 demonstrate the following as background pressure decreased: 1) broadening of the flux of high energy ions near centerline, 2) postponement of the appearance of low energy ions to larger angles, 3) an increase in the energy of low energy ions, and of course 4) a reduction in the number of low energy ions. The first feature is indicative of increased beam divergence, further evidence of which will be presented in the next section. The second feature may be at least in part due to increasingly steep radial potential gradients in the plume (top panels of Fig. 8), forcing slow ions out to higher angles as pressure decreased. The third feature, which is evident by observing variation in the position of the "RPA 20" curve between panels of Fig. 9, arises from increasing plasma potentials in the plume core (top panels of Fig. 8), where many slow ions are created. Note that the plasma potentials shown in Fig. 8 were recorded at a distance of 1 m from the thruster. Many slow ions were created closer to the thruster, where plasma potentials were presumably higher, but also where the variations in plasma potential with angle and background pressure may have been qualitatively similar to those shown in Fig. 8.

3. Ion energy

Figure 10 shows ion energy distributions (with respect to ground) recorded at L-3 with the RPA at a radius of 100 cm with an angular resolution of 5°. In discussion to follow, the "primary ion peak" refers to the prominent peak located at energy-to-charge ratios (E/q) near the discharge voltage of 300 V, and E/q_{max} refers to the value of E/q at the maximum of the primary ion peak. At angles less than or equal to 10° the data were adversely affected by high current density and the resultant accumulation of space charge within the probe, leading to an ion repelling field larger than the applied field, and a spurious shift of the primary peak to a lower-than-expected value of E/q.

Notable features of the data in Fig. 10 include: 1) the near invariance of E/q_{max} with angle and background pressure, 2) the appearance of primary ions at higher angles as pressure decreased, and 3) an increase in the energies of slow ions ($E/q \leq 50$ V) as pressure decreased. The variation of E/q_{max} is shown in Fig. 11, which plots E/q_{max} averaged over angles (excluding peaks with irregular shapes) as a function of background pressure. The typical standard deviation of E/q_{max} over angles at a given pressure was less than the voltage resolution of the RPA scan (2 V). At the highest background pressure (5.51E-5 Torr), a reasonably well-formed primary ion peak was detected out to a maximum of 85° from thruster centerline. At the lowest pressure (1.69E-6 Torr), primary ions were arguably detected out to 120°. The primary ion peak maxima from Fig. 10 are plotted as a function of background pressure in Fig. 12 for angles for which more than 3 data points (i.e., well-formed primary ion peaks) were available. Attenuation of primary ions with increasing background pressure was expected to occur, due to elastic collisions (including charge exchange) between ions and neutrals. At the average E/q_{max} of 255 V, the cross section for the $Xe^+ + Xe$ symmetric charge exchange (SCX) system is approximately 55×10^{-20} m^2.[22] Calculated values of the differential cross section for elastic scattering of 300 eV Xe^+ in Xe with and without charge exchange are presented in Ref. 23. By integrating those cross sections, we estimate that the total cross section for elastic scattering of primary ions is approximately 30% larger than the SCX cross section. The data of Fig. 12, along with the assumption that background neutral density was uniform and equal to the value measured by the ionization gauge, permit calculation of an effective cross section that would be required to explain the observed primary ion attenuation. This effective cross section is compared to the total elastic cross section in Fig. 13. It is evident that for angles greater than about 25°, elastic scattering is not sufficient to account for primary ion attenuation with increasing pressure, and that the attenuation rate increased with increasing angle, meaning that the thruster plume was actually becoming less divergent as pressure increased. Changes in plume divergence presumably indicate that the thruster electric field was modified, perhaps in a manner that shifted the regions of ionization and acceleration (the two are closely coupled in Hall thrusters, as evidenced by the invariance of E/q_{max} with background pressure) to a more downstream location as pressure decreased. Finally, the increasing energy of slow ions with decreasing background pressure confirms the trend of increasing plume plasma potentials observed in the Langmuir data (Section III.C.1).

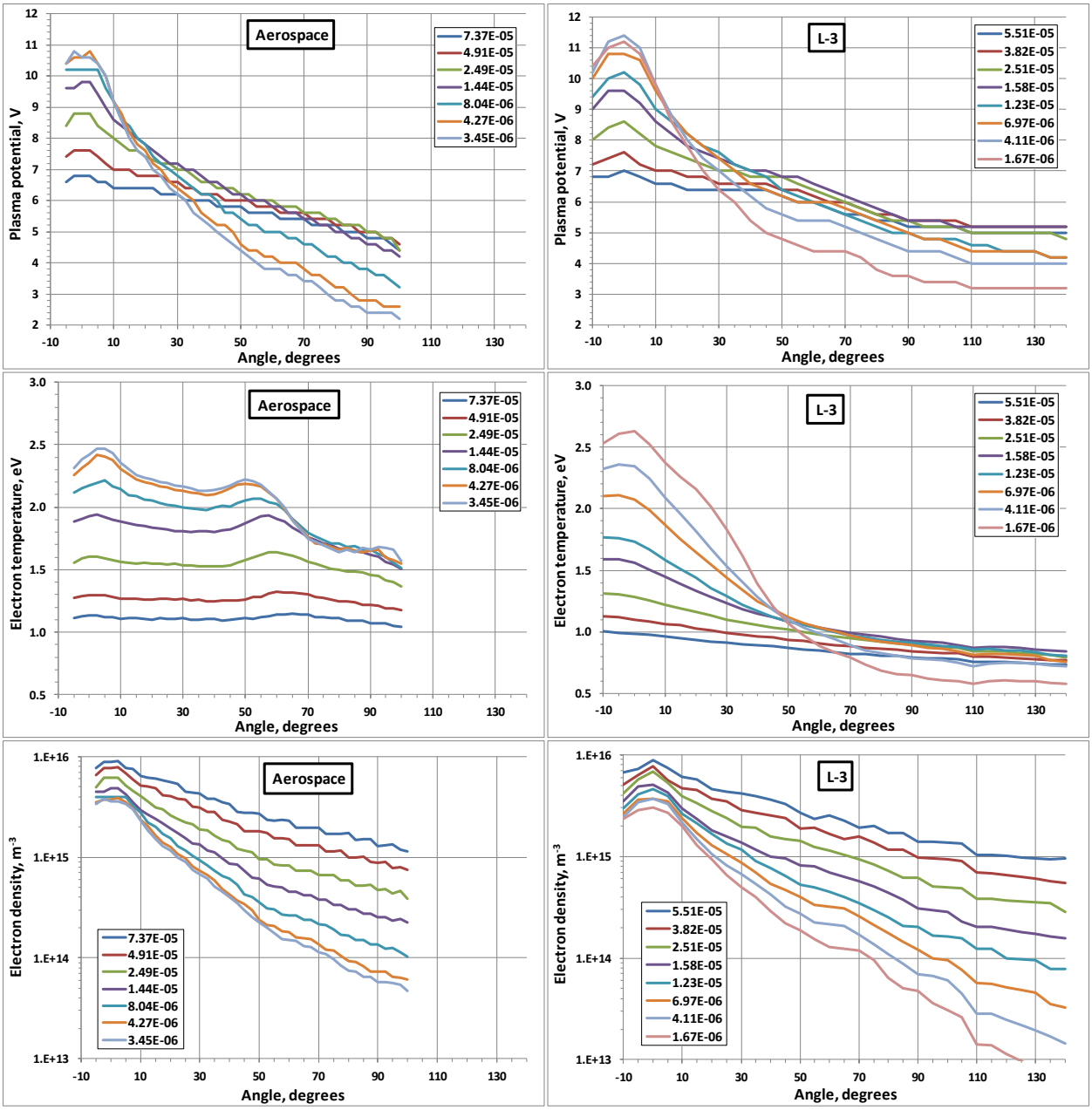

Figure 8. Langmuir probe results at 100 cm radius. Legends list background pressure in Torr.

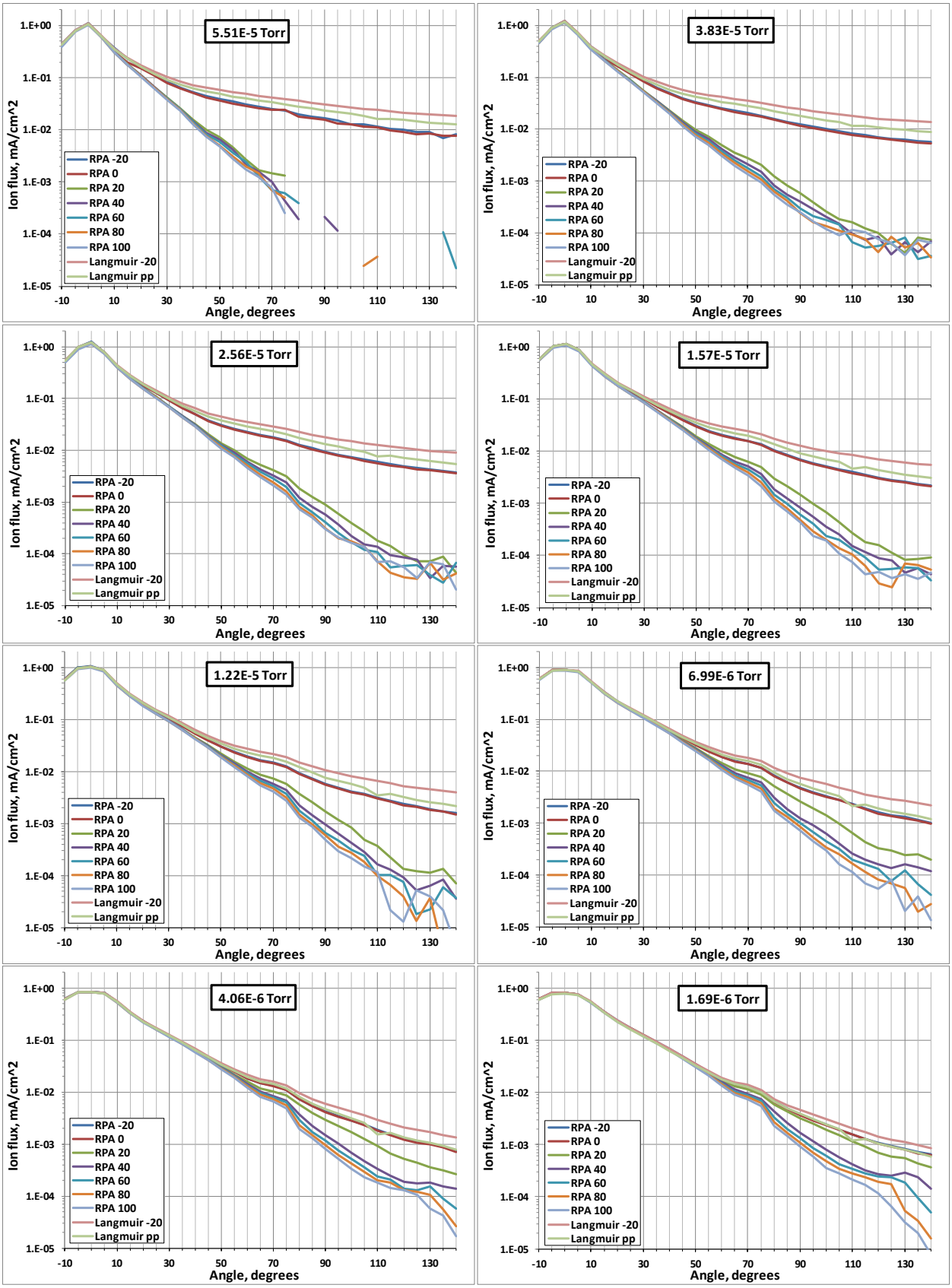

Figure 9. Ion flux measured at L-3 at 100 cm radius with RPA and Langmuir probes.

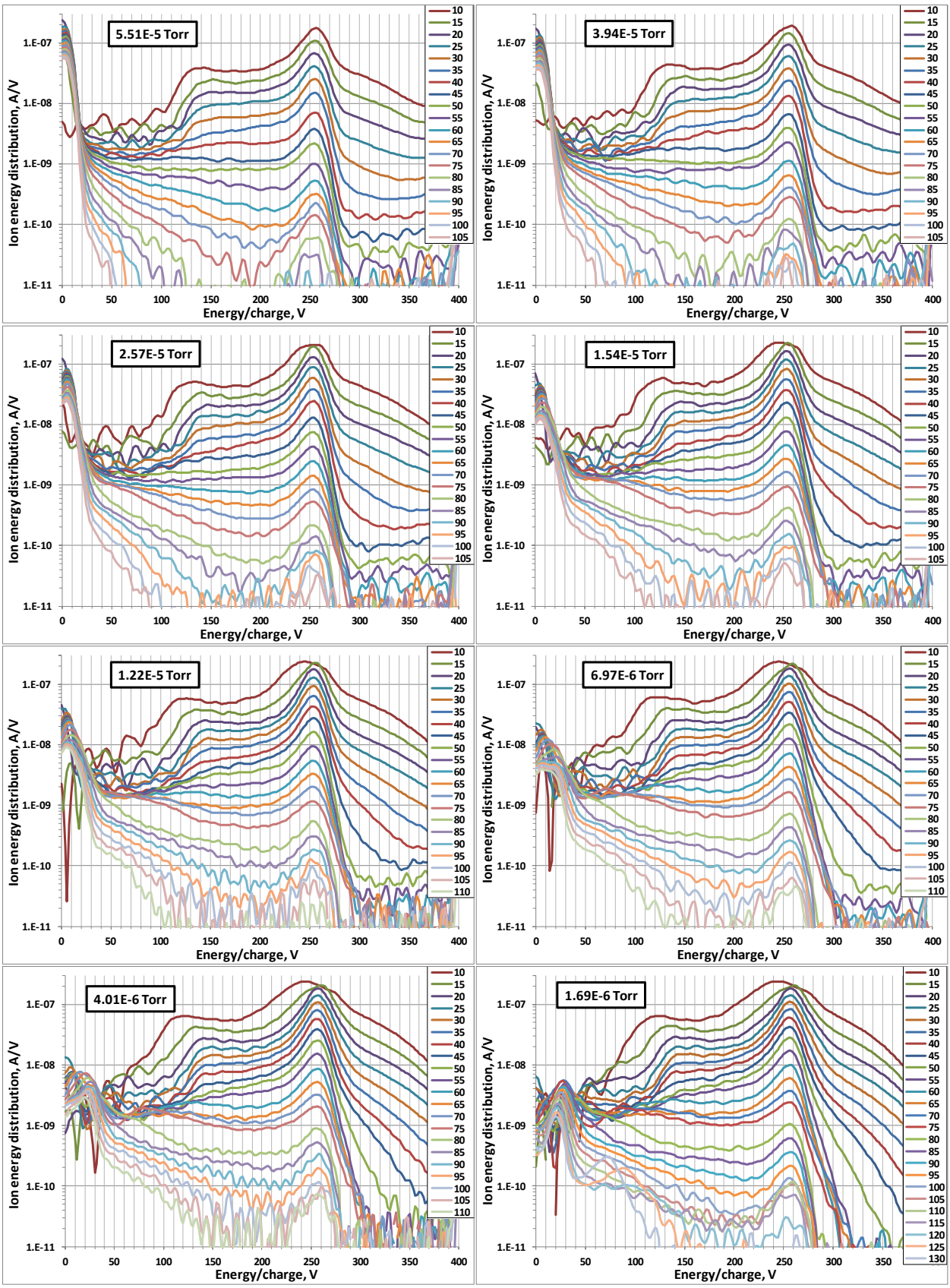

Figure 10. Ion energy distributions measured at L-3 at 100 cm radius with RPA (angles listed in legends).

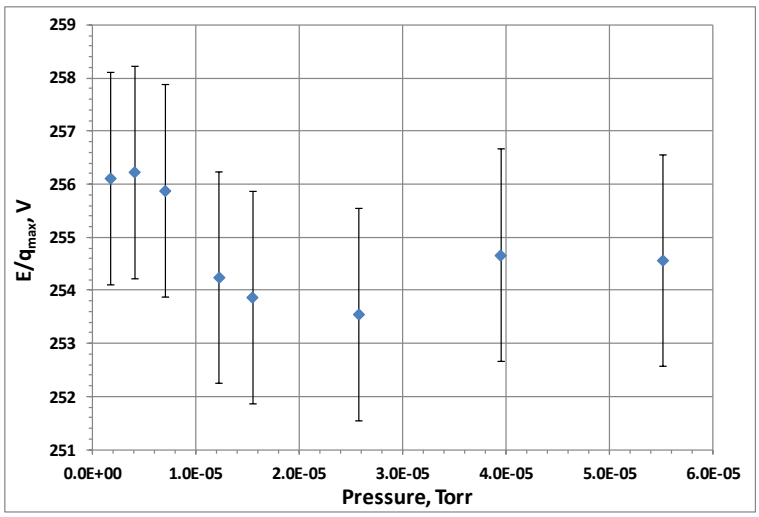

Figure 11. Energy-to-charge ratios at the primary ion peak maximum, averaged over angles.

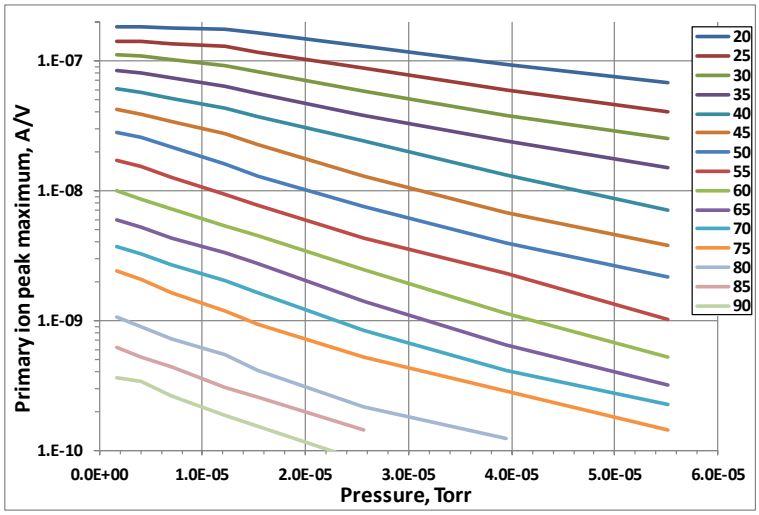

Figure 12. Primary ion peak maxima from the data of Fig. 11, angles listed in legend.

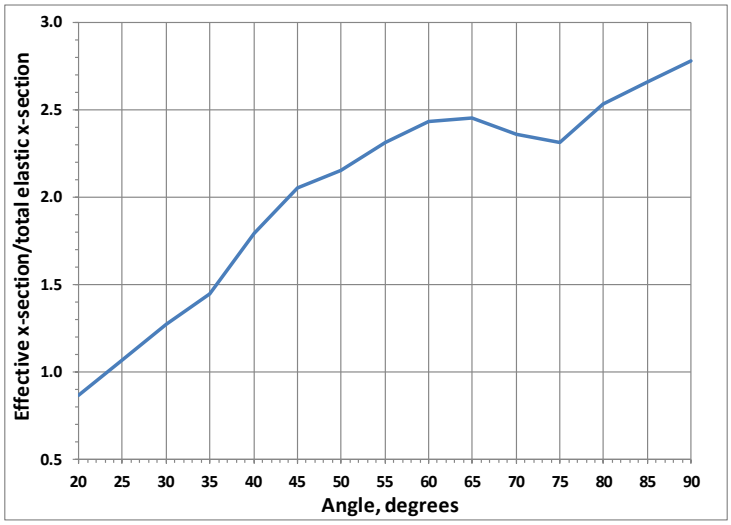

Figure 13. Ratio of "effective" scattering cross section needed to match the data of Fig. 13 to the total elastic (including charge exchange) cross section of the Xe^+, Xe system.

IV. Discussion

A. Role of background neutral density

Perhaps the most remarkable outcome of this investigation is that the performance data from the Aerospace and L-3 facilities agreed to within the accuracy of the measurements, despite differences in facility dimensions and thruster grounding (thruster body and thrust stand grounded at Aerospace, both floating at L-3). The same can be said in more qualitative fashion for the character of the discharge current oscillations. The elements that were common to the two facilities were the pressure gauge and its location relative to the thruster. It is tempting, therefore, to argue that background pressure, not some form of electrical interaction with the chamber or thruster mounting structure, is responsible for performance variation.

In 1993 Randolph et al.[24] suggested, based largely on testing of the SPT-100, that background pressures below 6.7×10^{-3} Pa (5.0×10^{-5} Torr) in ground testing are sufficient to obtain reliable predictions of in-orbit performance of Hall thrusters. This recommendation has gone largely unchallenged for the past two decades, but was recently revised down, without justification, to 4.0×10^{-3} Pa (3.0×10^{-5} Torr) in a "best practices" guide for electric propulsion testing.[25] Our data show that the performance of the SPT-100 not only continues to vary at background pressures below 3.0×10^{-5} Torr, but is actually the most sensitive to background pressure there.

The physical basis for this sensitivity is not well understood. The "simple ingestion" model, whereby propellant entrained from the vacuum chamber is treated as equivalent to propellant supplied to the thruster through the anode, clearly is not adequate to explain variations in thrust when discharge current is held constant. In addition, the total supplied flow rate varied by approximately 10% between the highest and lowest pressures studied. In contrast, the calculated rate of ingestion, based on free molecular flow through the exit plane at the pressure measured by the ionization gauge and an assumed background neutral temperature of 300 K, was 2.4% of the flow rate supplied to the anode at the highest pressure (0.05% at the lowest pressure). It is therefore necessary to assume an effective ingestion area approximately 4 times larger than the exit plane area to account for the observed variation in flow rate between the highest and lowest background pressures. This idea, however, presumes that the flow ingested through some boundary that extends well beyond the exit plane is ionized and accelerated in the same manner as if it had been supplied through the anode (since the extra flow required at reduced background pressure was supplied to the anode), which is very unlikely to be true.

A more relevant parameter to consider may be the ratio of the background neutral density to the neutral density somewhere in the discharge channel,[6,7] e.g., near the channel exit where the magnetic and electric fields are strongest and where most of the ionization occurs. Average neutral density at the exit plane of a low power laboratory model Hall thruster was estimated to be between 5×10^{17} and 4×10^{18} m^{-3} based on estimates of the mass utilization efficiency derived from plume data.[6] Neutral densities on channel centerline from numerical calculations performed on a BPT-4000 Hall thruster operating at 300 V and 4.5 kW dropped from 1×10^{18} to approximately 4×10^{16} m^{-3} between about 0.75L and L, where L is the channel length.[26] Neutral densities measured using two-photon laser-induced fluorescence 0.3 cm downstream of the exit plane of an SPT-140 Hall thruster operating at 300 V and 4.5 kW show considerable radial variation, ranging from a minimum of approximately 5×10^{17} m^{-3} on channel centerline to a maximum of approximately 8×10^{18} m^{-3} at the channel wall.[27] At a background pressure of 3×10^{-5} Torr (recommended by Ref. 25), and temperature of 300 K, the background neutral density is 1×10^{18} m^{-3}, implying that background neutrals are likely to play a dominant role, at least near channel centerline, in ionization and possibly conduction near the exit plane. By examining the optical emissions from the plume of an SPT-100, Manzella showed that background gas (nitrogen added to the vacuum chamber to raise the background pressure) was ingested and ionized.[28] That background neutrals affect the breathing mode ionization instability is evident from the data shown in the right-hand panel of Fig. 7.

B. Thrust loss mechanisms

It is relatively straightforward to identify two mechanisms for thrust loss based on the plume data contained in this report. The first has to do with the net ion accelerating voltage. Although Hall thrusters are often treated as electrostatic devices because ions are accelerated in a macroscopic electric field, the mechanism whereby momentum is transferred to the thruster structure is electromagnetic, and occurs through the magnetic field.[29,30] It may be inferred that once an ion has passed beyond a location, call it X_M, where the thruster magnetic field has dropped to a value that is negligible relative to the maximum field, any further acceleration experienced by that ion delivers negligible momentum to the thruster. Additional ion acceleration between the plume and grounded vacuum chamber occurs in ambipolar fields, and the momentum gained by the ions is communicated to the vacuum chamber by the electron pressure that supports those fields. Magnetic fields decay rapidly with distance, so X_M probably lies within 1 to 2 thruster diameters of the exit plane. The net ion accelerating voltage is the difference between *E/q*

measured by the ground-referenced RPA and the plasma potential (also ground-referenced) at X_M. Figure 11 shows that the primary ion E/q_{max} is invariant to within measurement uncertainty (2 V) over the full pressure range. We do not have plasma potential measurements within 1 to 2 thruster diameters of the exit plane, but those recorded at 100 cm (Fig. 8) show that plasma potential increased, albeit by the relatively small amount of 4 V near thruster centerline, with decreasing pressure. It is very likely that plasma potentials closer to the thruster also rose as background pressure decreased, resulting in reduced net ion accelerating voltages and a loss of thrust (in proportion to the square root of the net accelerating voltage). A change of 4 V out of 255 V will change thrust by only 0.8%, so this mechanism is not likely to be the dominant cause of thrust reduction.

The second thrust loss mechanism is plume divergence. We observed broadening of the ion flux near centerline (Fig. 9), and increasing prominence of primary ions at higher angles (inferred from Figs. 10, 12, and 13), as pressure decreased.

In principle it is possible to calculate thrust from plume data, however in practice it is very difficult to do so with an accuracy approaching that available from direct thrust measurements. Nevertheless, we will make the attempt in order to see if the mechanisms just discussed can reproduce the thrust variation shown in Fig. 6. A large number of assumptions and approximations, the validity of which cannot all be verified at present, are required to do so, as detailed in the following paragraphs.

The first approximation is that thrust is equal to just the momentum flux integrated across a surface downstream of the thruster, with no contribution from pressure (presumably primarily due to electrons) acting at the surface. Ideally, the momentum flux at a given angle should be calculated from integration over the ion energy distribution function (IEDF), with separate IEDFs measured for each charge state. We did not measure IEDFs vs. charge state, and the IEDFs that we have are heavily modified by interactions with background neutrals. As an alternative, we will treat the ions as a fluid with a bulk average velocity v calculated from the difference between the average value of E/q_{max} (255 V, see Section III.C.3) and the plasma potential measured at 100 cm. In this case we can write the following expression for thrust F:

$$F = \iint \rho \vec{v}\vec{v} \cdot d\vec{A} \tag{4}$$

where ρ is the mass density, $\vec{v}$ is the velocity vector, and $d\vec{A}$ is the unit vector normal to area element dA. If we further assume azimuthal symmetry, that the ion current vector is parallel to $d\vec{A}$ (the so-called "point source" assumption), that we are only interested in the component of thrust along the thruster axis (the component sensed by the thrust stand), that the fractional currents of multiply charged ions do not vary with angle from thruster centerline (Kim and Gallimore[31] measured multi-charged ion fractions in the plume of an SPT-100 at a background pressure of 4.2×10^{-5} Torr and found them to be weakly dependent on angle from thruster centerline), and if we ignore numerical constants, Eq. 4 becomes:

$$F \propto \int v J_{primary} \cos\theta \sin\theta d\theta \tag{5}$$

where $J_{primary}$ is the current of primary ions at angle θ from thruster centerline. We will obtain $J_{primary}$ from the current collected by the RPA at a repelling bias of 100 V (J_{RPA100}). It is necessary to correct J_{RPA100} for losses due to elastic scattering (including charge exchange) using an expression of the form:

$$J_{primary} = J_{RPA100} \exp(R/\lambda) \tag{6}$$

where R is the distance to the RPA (1 m) and λ is the scattering mean free path. Using λ calculated from an assumed uniform neutral background density and total elastic cross-section of 72×10^{-20} m^2 (Section III.C.3), and integrating according to Eq. 7, the current utilization efficiencies η_c (ratio of plume ion current to discharge current J_D) shown in Fig. 14 under the heading "RPA100" were obtained.

$$\eta_c = \frac{2\pi R^2}{A J_D} \int J_{primary} \sin\theta d\theta \text{ ; } A = \text{RPA collector area} \tag{7}$$

Also shown in Fig. 14 are values of η_c calculated from ion fluxes obtained by extrapolating Langmuir probe ion saturation currents to plasma potential (Section II.C.3). Both methods returned values of η_c greater than 1 at the highest pressure, which is a non-physical result. Sources of error for the RPA-derived estimates may include sheath expansion (i.e., expansion of the effective area for ion collection) and non-uniformity of the neutral background density. For the Langmuir probe, extrapolation of ion saturation current to plasma potential presumably minimizes error associated with sheath expansion since there is no sheath when the probe is at plasma potential, however there is no theory that demonstrates that a linear extrapolation is valid all the way to plasma potential, and it is likely that the error associated with the linear extrapolation will increase as the population of low-energy ions increases, due to their relatively greater susceptibility to sheath expansion effects. The Langmuir probe does not discriminate based on ion energy, and collects slow ions generated from charge exchange and elastic scattering of primary ions with background neutrals. It is appropriate to count those ions when calculating η_c, however the Langmuir probe will also collect slow ions created by electron-impact ionization of background neutrals, which should not be counted and will artificially increase η_c. The Langmuir probe also has a 180° angular acceptance, and will collect slow ions originating from the extended source volume extending well downstream of the thruster, in violation of the point source assumption. Both probes are susceptible to error associated with secondary electron emission by ion bombardment, however this effect is primarily dependent on the ion charge state distribution and is not likely to be very sensitive to background pressure. For the reasons listed above, we consider the values of η_c calculated at the lowest pressures to be the most accurate. We will now assume that η_c is invariant with background pressure and equal to 0.85, which is the averge of the RPA and Langmuir-derived values over the five lowest pressures. There is no justification for this assumption, other than it improved the agreement between calculations of normalized thrust and our measurements. Under this assumption, our procedure for calculating $J_{primary}$ became to assign a value for λ such that the integration shown in Eq. 7 yielded $\eta_c = 0.85$. For all but the lowest pressure, the assigned value of λ differed by less than 15% from the value calculated using the total elastic cross section and an assumed uniform background density.

A comparison between thrusts calculated from Eq. 5 and values measured with the thrust stand is shown in Fig. 15. Both calculated and measured thrusts are normalized by their maximum value. Complete sets of probe data were not available to calculate thrust at the two highest pressures. By ignoring the presence of multicharged ions in our calculation of normalized thrust, we implicitly assumed that the current fractions of multicharged ions were not only invariant with angle as previously mentioned, but also with background pressure. Given the large number of assumptions and approximations detailed above, it is not feasible to assign uncertainties to calculated thrust, rendering this exercise somewhat academic. However, it appears plausible that the decline in thrust with decreasing background pressure was primarily due to increased beam divergence, with a smaller contribution from decreased net ion accelerating voltage.

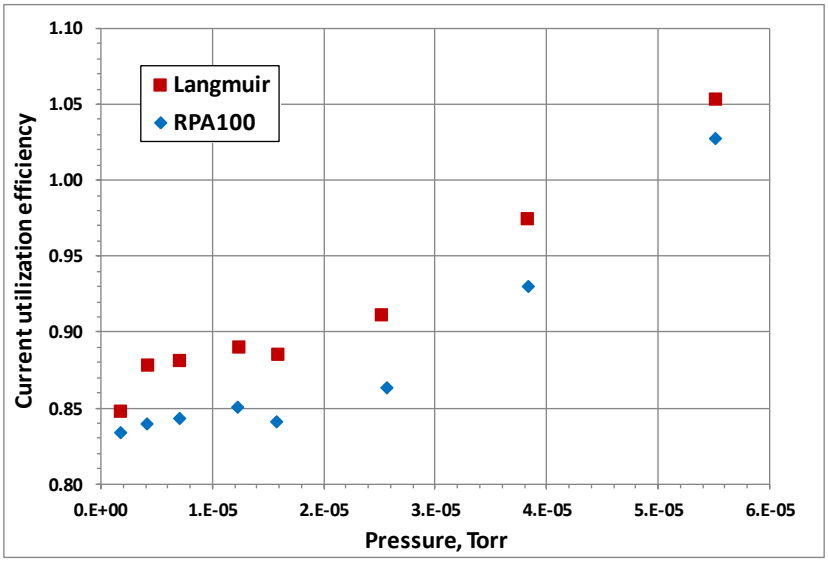

Figure 14. Current utilization efficiencies derived from Langmuir probe and RPA (repelling bias of 100 V).

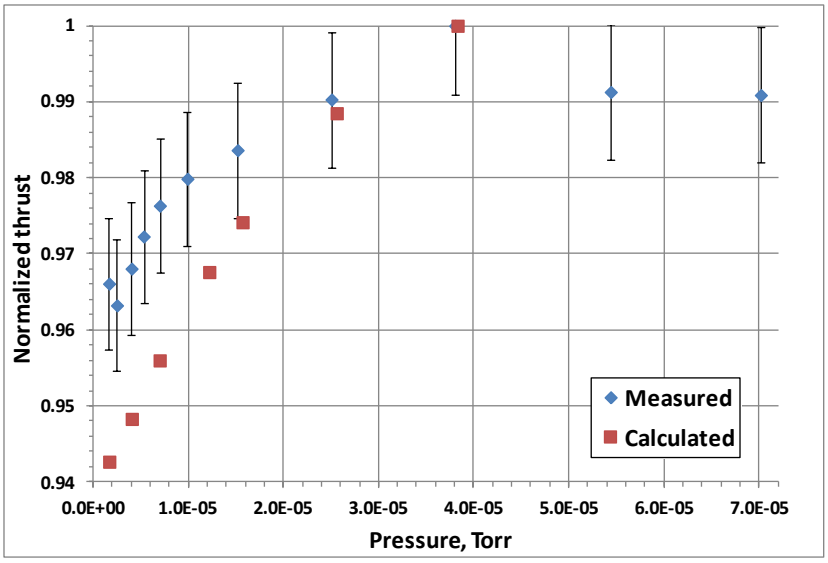

Figure 15. Normalized thrust, measured with the thrust stand, and calculated from Eq. 5.

V. Conclusion

A flight-model SPT-100 Hall thruster from the Fakel Experimental and Design Bureau was characterized with respect to performance and plume properties at The Aerospace Corporation (Aerospace) and at L-3 Electron Technologies, Inc. (L-3) over vacuum facility background pressures ranging from 2.3×10^{-4} to 9.5×10^{-3} Pa (1.7×10^{-6} to 7.1×10^{-5} Torr). The same pressure gauge mounted in the same location relative to the thruster was used to measure background pressures in both facilities. The same thrust stand was also used in both facilities, although the thruster mounting structure and thrust stand were electrically grounded at Aerospace and left floating at L-3. Thrust and xenon mass flow rates measured at both facilities agreed to within the measurement uncertainties. Thrust decayed exponentially, while flow rate increased linearly, with decreasing pressure. Using simple curve-fits to extrapolate to zero pressure, thrust, specific impulse, efficiency, and flow rate were projected to change by -4, -10, -14, and 7% respectively relative to values at 6.7×10^{-3} Pa (5.0×10^{-5} Torr). Increased plume divergence was identified as the dominant contributor to decreased thrust with decreasing pressure, with a smaller contribution from decreased net ion accelerating voltage. Increased plume divergence is presumably indicative of a modified electric field, perhaps resulting in movement of the ionization and acceleration zones to a more downstream location. The amplitude of discharge current oscillations presumed to derive from the "breathing" mode ionization instability decreased linearly with decreasing background pressure, while the center frequency of the oscillations also decreased, but in non-linear fashion. It was noted that neutral density near the exit plane of Hall thrusters can be quite low, such that background neutrals from the residual gas in the vacuum chamber may significantly influence ionization and conduction there. Presumably thrusters designed to produce higher exit plane neutral densities would be less sensitive to background pressure, however other design choices may also influence pressure sensitivity. The Hall thruster user community would benefit from an understanding of how various design choices affect pressure sensitivity, so that thrusters can be designed to perform the same in space as they do in affordable ground-test facilities.

Acknowledgments

Contributors to this project included Mike Worshum, Byron Zeigler, Kevin Dorman, and Jason Young of The Aerospace Corporation; Dan Katz of SSL; and Sam Sawyer, Mike McKenna, Gary Wise, Larry Martin, and Winston Thompson of L-3 ETI. The authors benefited from discussions with Mark Smith and Mark Crofton of The Aerospace Corporation.

References

[1]Byers, D. and Dankanich, J.W., "A Review of Facility Effects on Hall Effect Thrusters," IEPC 2009-076.

[2]Sankovic, J.M., Hamley, J.A., and Haag, T.W., "Performance Evaluation of the Russian SPT-100 Thruster at NASA LeRC," IEPC 93-094.
[3]Sankovic, J.M., Haag, T.W., and Manzella, D.H., "Performance Evaluation of a 4.5 kW SPT Thruster," IEPC 95-30.
[4]Hofer, R.R., Peterson, P.Y., and Gallimore, A.D., "Characterizing Vacuum Facility Backpressure Effects on the Performance of a Hall Thruster," IEPC 2001-045.
[5]Nakles, M.R. and Hargus, W.A., "Background Pressure Effects on Internal and Near-field Ion Velocity Distribution of the BHT-600 Hall Thruster," AIAA 2008-5101.
[6]Diamant, K.D., Spektor, R., Beiting, E.J., Young, J.A., and Curtiss, T.J., "The Effects of Background Pressure on Hall Thruster Operation," AIAA 2012-3735.
[7]Hargus, W.A., Tango, L.J., and Nakles, M.R., "Background Pressure Effects on Krypton Hall Effect Thruster Internal Acceleration," IEPC 2013-F.
[8]Huang, W., Kamhawi, H., and Haag, T., "Effect of Background Pressure on the Performance and Plume of the HiVHAc Hall Thruster," IEPC 2013-058.
[9]Pidgeon, D.J., Corey, R.L., Sauer, B., and Day, M.L., "Two Years On-Orbit Performance of SPT-100 Electric Propulsion," AIAA 2006-5353.
[10]Tverdokhlebov, S.O., et al., "Overview of Russian Electric Propulsion Activities," AIAA 2002-3562.
[11]Poussin, J.-F. and Berger, G., "Eurostar E3000 Three-Year Flight Experience and Perspective," AIAA 2007-3124.
[12]Corey, R.L., Gascon, N., Delgado, J.J., Gaeta, G., Munir, S., and Lin, J., "Performance and Evolution of Stationary Plasma Thruster Electric Propulsion for Large Communications Satellites," AIAA 2010-8688.
[13]Casaregola, C., "Electric Propulsion for Commercial Applications: In-Flight Experience and Perspective at Eutelsat," IEPC 2013-332.
[14]Brophy, J.R., "Stationary Plasma Thruster Evaluation in Russia," NASA CR-192823, 1992.
[15]Randolph, T., Bekrev, M., Day, M., Fischer, G., Koriakin, A., Kozubsky, K., Krochak, L., Maslennikov, N., Pidgeon, D., Pridannikov, S., Rogers, W., Staley, M., and Yuriev, A., "Integrated Test of an SPT-100 Subsystem," AIAA 97-2915.
[16]Gnizdor, R., Kozubsky, K., Koryakin, A., Maslennikov, N., Pridannikov, S., and Day, M., "SPT100 Life Test with Single Cathode up to Total Impulse Two Million Nsec," AIAA 98-3790.
[17]Sankovic, J.M., Hamley, J.A., and Haag, T.W., "Performance Evaluation of the Russian SPT-100 Thruster at NASA LeRC," IEPC 93-094.
[18]Garner, C.E., Brophy, J.R., Polk, J.E., Pless, L.C., and Starling, D.A., "A 5730-Hr Cylcic Endurance Test of the SPT-100," IEPC 95-179.
[19]Chien, K.-R., Tighe, W.G., Bond, T.A., and Spears, R., "An Overview of Electric Propulsion at L-3 Communications, Electron Technologies Inc." AIAA 2006-4322.
[20]Choueiri, E.Y., "Plasma Oscillations in Hall Thrusters," Physics of Plasmas, Vol. 8, No. 4, April 2001, pp. 1411-1426.
[21]Pollard, J.E., and Diamant, K.D., "Hall Thruster Plume Shield Wake Structure," AIAA 2003-5018.
[22]Miller, J.S., Pullins, S.H., Levandier, D.J., Chiu, Y., and Dressler, R.A., "Xenon Charge Exchange Cross Sections for Electrostatic Thruster Models," Journal of Applied Physics, Vol. 91, No. 3, February 2002, pp. 984-991.
[23]Boyd, I.D. and Dressler, R.A., "Far Field Modeling of the Plasma Plume of a Hall Thruster," Journal of Applied Physics, Vol. 92, No. 4, August 2002, pp. 1764-1774.
[24]Randolph, T., Kim, V., Kaufman, H., Kozubsky, K., Zhurin, V., and Day, M., "Facility Effects on Stationary Plasma Thruster Testing," IEPC 1993-093.
[25]Dankanich, J.W., Walker, M., Swiatek, M.W., and Yim, J.T., "Recommended Practice for Pressure Measurements and Calculation of Effective Pumping Speeds during Electric Propulsion Testing," IEPC 2013-358.
[26]Mikellides, I.G., Katz, I., Hofer, R.R., and Goebel, D.M., "Hall-Effect Thruster Simulations with 2-D Electron Transport and Hydrodynamic Ions," IEPC 2009-114.
[27]Crofton, M.W., Hsu-Schouten, A.G., Young, J.A., Beiting, E.J., Diamant, K.D., Corey, R.L., and Delgado, J.J., "Neutral Xenon Density in the SPT-140 Near-Field Plume," IEPC 2013-399.
[28]Manzella, D.H., "Stationary Plasma Thruster Plume Emissions," IEPC 93-097.
[29]Jahn, R.G., *Physics of Electric Propulsion*, McGraw-Hill, 1968, Chap. 8.
[30]Goebel, D.M. and Katz, I., *Fundamentals of Electric Propulsion, Ion and Hall Thrusters*, John Wiley and Sons, 2008, p. 21.
[31]Kim, S.-W. and Gallimore, A.D., "Plume Study of a 1.35 kW SPT-100 Using an ExB Probe," Journal of Spacecraft and Rockets, Vol. 39, No. 6, November-December 2002, pp. 904-909.